# *Exploring the Coherent Structure of Dynamic Systems through POD and DMD Methods*


## ABSTRACT

This project includes mathematical derivations and applications of Proper Orthogonal Decomposition (POD) and Dynamic Mode Decomposition (DMD) methods for studying dynamic systems. The primary focus involves the application of these methodologies to analyze the flow field in a fluid dynamic system, with the objective of capturing coherent structures through POD and DMD modes. The investigation also provides visualization of the underlying dynamics structures, such as plots for POD modes and the associated energy spectrum, as well as DMD modes and eigenvalues. For a specific snapshot, a detailed analysis of Pearson's correlation coefficient is conducted, comparing the accuracy of POD approximation and DMD reconstruction with the original data. Additionally, the study presents the comparative assessment of data distributions through scatter graphs, individually contrasting POD approximation and DMD reconstruction with the original data. The findings are encapsulated in a respective comparison of reduced-rank POD approximation and reduced-dimensional DMD reconstruction with the original data at a specific snapshot of the studied system.


## Introduction

The model for this project is a two-dimensional flow past a circular cylinder, and the axis of the cylinder is parallel to the z-axis. Generally, collecting data about the flow field requires recording the velocity at different locations $(x, y)$ over time. The measurement of the fluid flow was done on a grid $n_x \times n_y$ (768 x 192) at a time step of 0.125 seconds. The vorticity of the flow is defined as the curl of the velocity vector ($v$): $w = \nabla \times v$. The data for this project is organized as a matrix, where each row corresponds to a point in space, and each column corresponds to a snapshot in time. Each snapshot of the data is the z-component of the vorticity field ($w_z$), stored as a vector of length $n_x \times n_y$ (768 x 192). The following figure visualizes the flow in two snapshots, where $w_x$ has been represented in red (positive values), blue (negative values), and white (nearly zero values).

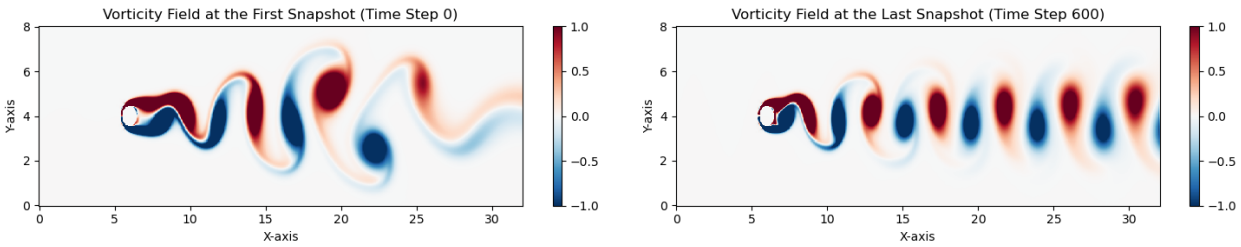


**Figure 1: The Vorticity Field of the flow past a cylinder in two snapshots.**

In a flow field, the coherent structure is organized and repeating patterns of motion, such as vortices. Our goal is to identify and extract coherent components, which involves recognizing patterns that maintain their integrity in a fluid flow. This can be done through the application of decomposition methods like Proper Orthogonal Decomposition (POD) and dynamic mode decomposition (DMD). POD or DMD can decompose the flow field into spatially and temporally coherent modes, making it easier to identify and analyze these structures.

# Methodology

## The Proper Orthogonal Decomposition (POD)

The Proper Orthogonal Decomposition (POD) is a mathematical method that takes the collected high-dimensional data and breaks it down into a set of modes. These modes represent the dominant patterns or structures in the flow. Because these modes are orthogonal, they are uncorrelated or independent of each other, meaning each mode captures a distinct spatial pattern of flow. The modes are ordered by energy content, allowing for the identification of dominant coherent structures.

Suppose the matrix $U$ contains the measured fluid data (z-component of vorticity field):

$$U_{ij} = w_z(\vec{x}_i, t_j),\ where\ the\ length\ of\ \vec{x}\ is\ n = n_x \times n_y$$

Assume the vorticity field was computed or measured in $n$ discrete grid, and $m$ snapshots of these flow fields are collected at various time steps $t_1, t_2, \ldots, t_m$. The vorticity field data at time $t_k$ denoted by the column vector $\vec{u}_k = u(t_k) = w_z(\vec{x}, t_k) \in R^n$, so that the data matrix $U \in R^{n \times m}$ is formed by arranging the column vectors $\vec{u}_k$ as following:

$$U = \begin{bmatrix} | & | & ... & | \\ \vec{u}_1 & \vec{u}_2 & ... & \vec{u}_m \\ | & | & ... & | \end{bmatrix}$$

The vorticity field snapshot $\vec{u}$ can be approximated by a linear combination of a set of suitable orthogonal basis $\{\phi_k\}$, where $\phi_k \in R^m$:

$$\vec{u}(\vec{x}, t) = \sum_{k=1}^{n} \phi_k(\vec{x})\vec{c}_k(t)$$

or equivalently, for time step $t = t_j$, j-th snapshot of $U$:

$$\vec{u}_j = \sum_{k=1}^{n} \vec{\phi}_k c_{kj}$$

To obtain such basis, referred to as POD modes, the process relies on performing Singular Value Decomposition (SVD) of $U \in R^{n \times m}$:

$$U_{n \times m} = \Phi_{n \times n} \Sigma_{n \times m} \Psi^T_{m \times m}$$

The columns of $n \times n$ matrix $\Phi$ are POD modes with the same dimensional as each snapshot of $U$. The singular values in $\Sigma$ represent the amount of energy captured by each mode. The modes in columns of $\Phi$ and raws of matrix $\Psi^T$ capture spatial and temporal patterns, respectively. Additionally, the columns of $\Phi$ and $\Psi$ are orthogonal, so $\Phi\Phi^T = I_n, \Psi\Psi^T = I_m$. The following graph shows the singular values produced by decomposing 200 snapshots of $U$, providing insights into the dominant modes captured by SVD:

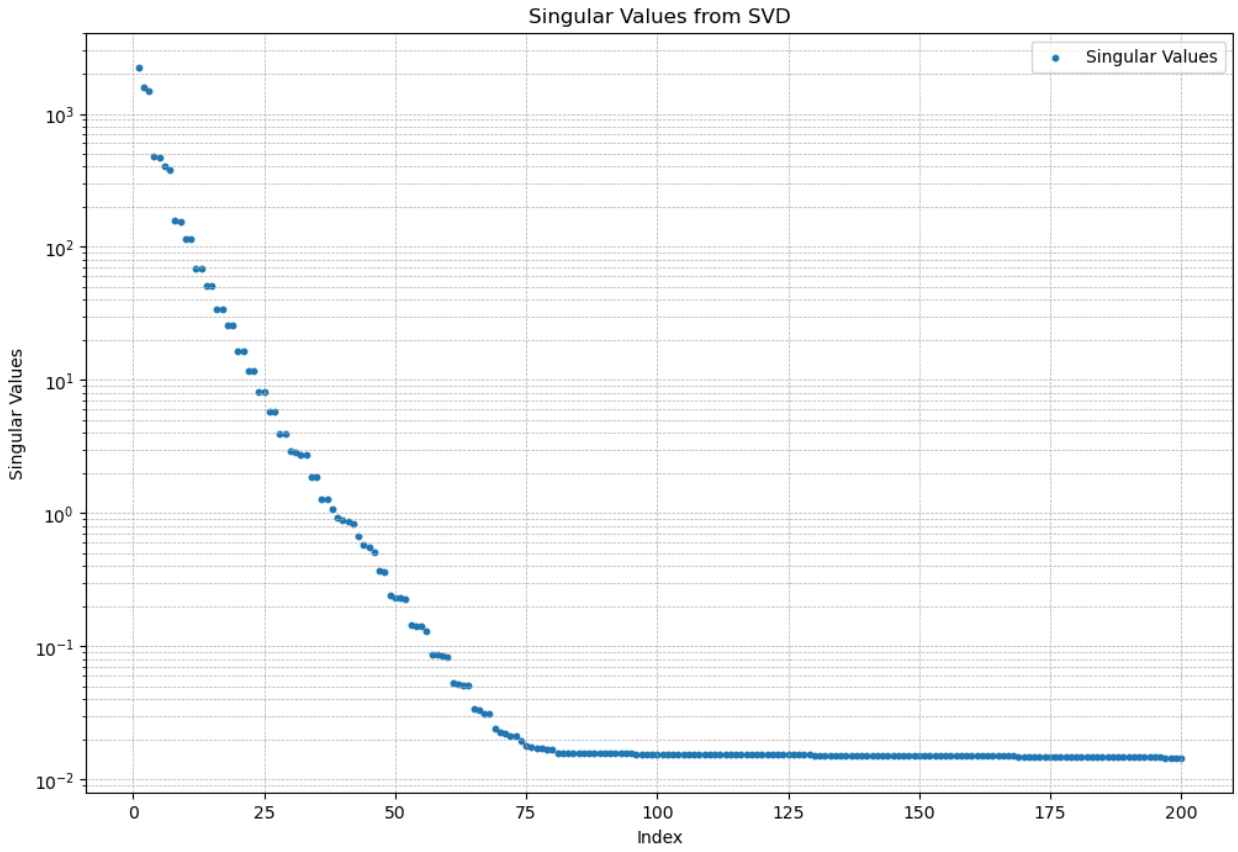


**Figure 2: Plot of the 200 singular values in Σ, illustrating the distribution of energy.**

As the importance of each POD mode is determined by the corresponding singular value, visualizing the first 6 dominant modes provides insights into the spatial patterns that contribute to the underlying dynamics:

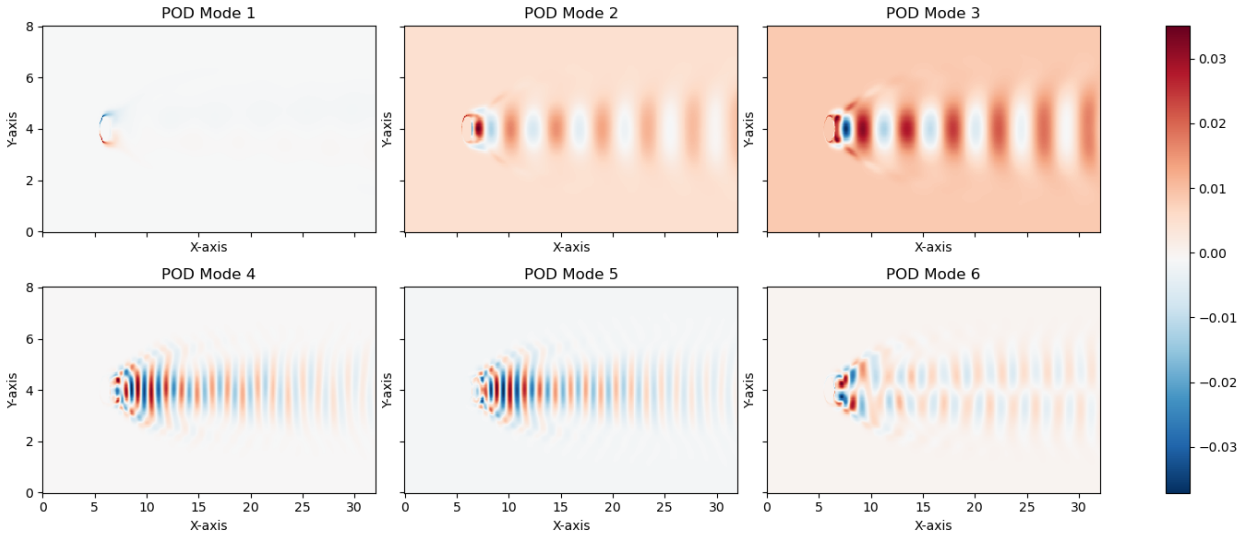


**Figure 3: Visualization of the First Six POD Modes. The subplots display the spatial patterns of each POD mode and the color represents the amplitude of the modes.**

According to the Eckart-Young-Mirsky (EYM) theorem, the best rank-$r$ approximation to a matrix $U \in R^{n\times m}$, where $min\{n, m\} \geq r$, is obtained by taking first $r$ components of the SVD of $U$. Denote such rank-$r$ approximation matrix as $r\_U$, and take the first $r$ columns of matrix $\Phi_{n\times n}$ and $\Psi_{m\times m}$:

$$r\_U_{n\times m} = \Phi_{n\times r}\Sigma_{r\times r}\Psi^T_{r\times m}$$

The EYM theorem then states for all possible rank-$r$ matrix, $r\_U$ is the best approximation of $U$ in a lest-square sense. After truncating all but the first $r$ dominant modes, the j-th vorticity field snapshot can be approximated by a linear combination of the $r$ modes:

$$\vec{u}_j \approx \sum_{k=1}^{r} \vec{\phi}_k c_{kj} = \sum_{k=1}^{r} \vec{\phi}_k \sigma_k \Psi^T_{kj}$$

where POD mode $\phi_k$ is the k-th column of matrix $\Phi_{n\times r}$, $\sigma_k$ is the k-th singular value in diagonal matrix $\Sigma_{r\times r}$, and $\Psi^T_{kj}$ is the entry in the k-th row and j-th column of the matrix $\Psi^T_{r\times m}$, representing the time coefficients associated with the k-th POD mode.

Observing the dominant singular values from Figure 2, it is proper to choose rank-7 approximation to matrix U. The following scatter plot shows the values from one snapshot (at time-step 500) of the original data matrix $U$ against the corresponding snapshot from the column of the rank-7 approximation matrix $r\_U$ :

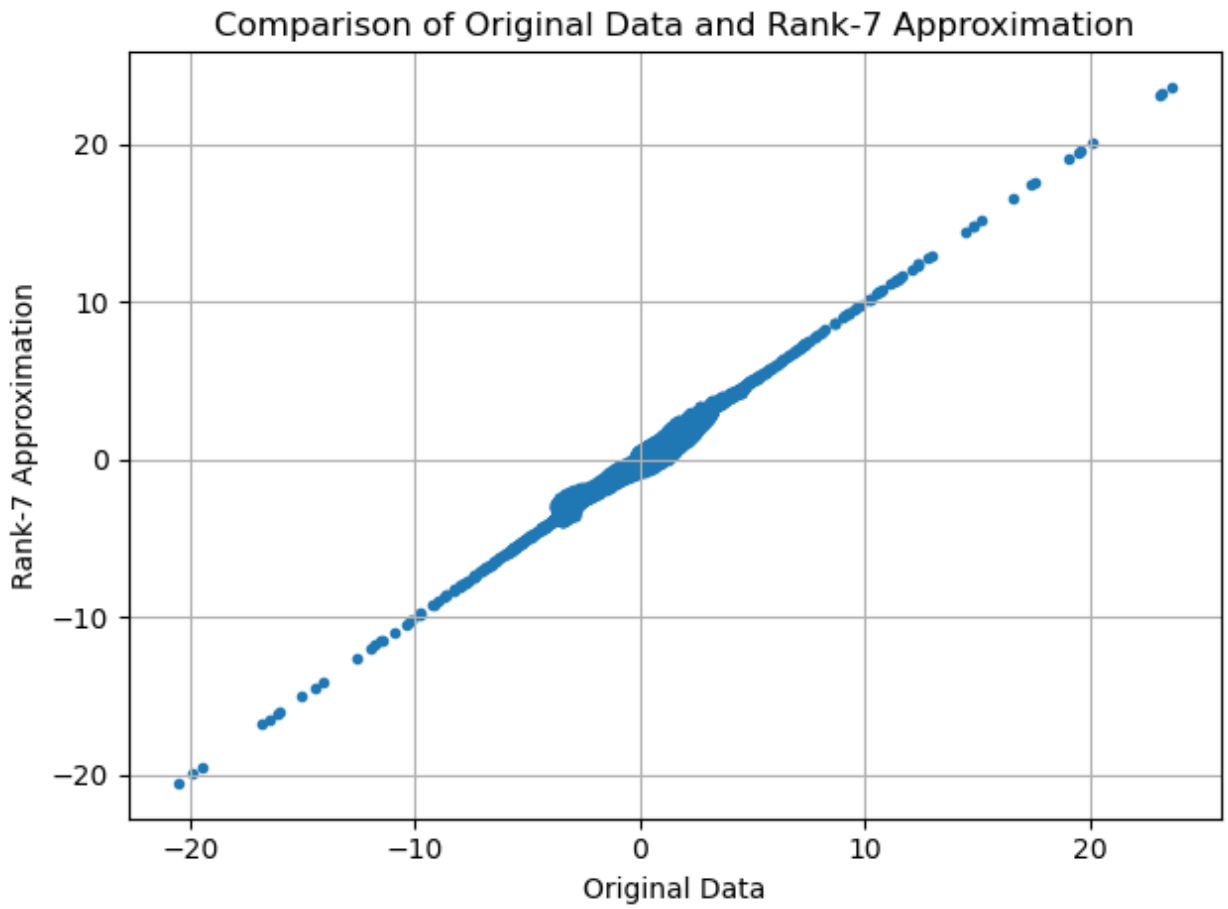


**Figure 4: Original Data vs. Rank-7 Approximation at Time-Step 500**

To quantify the agreement between the original and approximated values, need to compute Pearson's correlation coefficient. The formula for calculating Pearson's correlation coefficient $(r_p)$ between two variables X and Y with n data points is as follows:

$$r_p = \frac{\sum_{i=1}^{n}(X_i - \bar{X})(Y_i - \bar{Y})}{\sqrt{\sum_{i=1}^{n}(X_i - \bar{X})^2 \sum_{i=1}^{n}(Y_i - \bar{Y})^2}}$$

The result for computing $r_p$ between the original data $U$ and rank-7 approximation $rU$ at 500-th snapshot is 0.9950573, which is close to 1, indicating a strong positive correlation, meaning that $rU$ well captured the key pattern in the original data.

The following figure visualizes the vorticity field obtained by the snapshot of $U$ and $rU$ respectively:

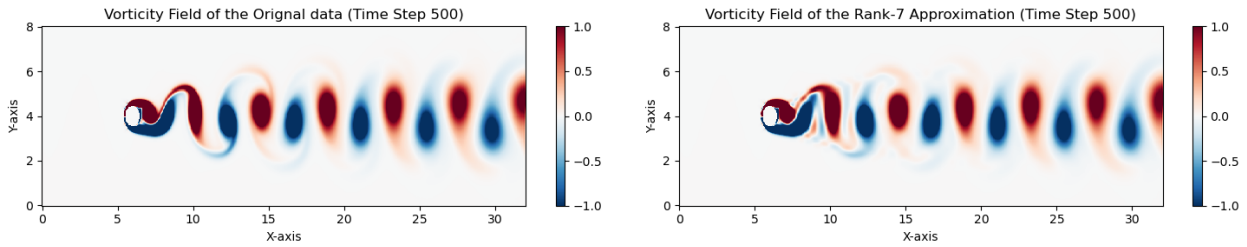


**Figure 5: Comparison of Vorticity Fields of the Original Data and POD Approximation at 500-th Snapshot**

# Dynamic Mode Decomposition (DMD)

DMD is another decomposition technique that simultaneously identifies spatially coherent modes that are constrained to have the same linear behavior in time, given by oscillations at a fixed frequency with growth or decay. Thus, DMD follows a linear model of a set of dimensionally reduced spatial modes along with their temporal evolution, which is different from POD modes that only capture spatial patterns.

To derive the formulation DMD, the snapshots in the original data matrix $U \in R^{n \times m}$ are spaced evenly in time, so that $t_k = t_1 + (k-1)\Delta t$, with $\Delta t$ sufficiently small to resolve the highest frequencies in the dynamics. Assume the first snapshot is at $t_1 = 0$, then $t_k = (k-1)\Delta t$. DMD aims to find the leading eigenvalues and eigenvectors of the linear operator $A$ that evolves snapshots forward in time:

$$\vec{u}_k \approx A\vec{u}_{k-1}$$

In practice, this linear operator is identified by first splitting the data matrix $U$ into two matrices:

$$U_{m-1} = \begin{bmatrix} | & | & \dots & | \\ \vec{u}_1 & \vec{u}_2 & \dots & \vec{u}_{m-1} \\ | & | & \dots & | \end{bmatrix} \qquad U_m = \begin{bmatrix} | & | & \dots & | \\ \vec{u}_2 & \vec{u}_3 & \dots & \vec{u}_m \\ | & | & \dots & | \end{bmatrix}$$

and then solving for the operator $A$ that satisfies:

$$U_m \approx AU_{m-1}$$

via the following least-squares optimization problem:

$$A = \arg\min_A \|U_m - AU_{m-1}\|_F = U_m U_{m-1}^{\dagger}$$

where $\| \ . \ \|_F$ is the Frobenius norm and $U_{m-1}^{\dagger}$ is pseudo-inverse matrix of $U_{m-1}$, which can be obtained by performing POD:

$$U_{m-1} = \Phi_{n\times n}\Sigma_{n\times(m-1)}\Psi^T_{(m-1)\times(m-1)} \approx \Phi_{n\times r}\Sigma_{r\times r}\Psi^T_{r\times(m-1)}$$

For convenience, denote matrix $\Phi_{n\times r}$, $\Sigma_{r\times r}$, and $\Psi^T_{r\times(m-1)}$ as $\Phi_r$, $\Sigma_r$, and $\Psi^T_r$ respectively, so that

$$U_{m-1}^{\dagger} \approx \Psi_r\Sigma_r^{-1}\Phi_r^T$$

Now the linear operator $A$ can be approximated by:

$$A \approx U_m\Psi_r\Sigma_r^{-1}\Phi_r^T$$

In practice, the matrix $A$ is too large to analyze directly, and instead, project $A$ into $r$-dimensional POD subspace:

$$\tilde{A} = \Phi_r^T A\Phi_r = \Phi_r^T U_m\Psi_r\Sigma_r^{-1}$$

Also, perform eigendecomposition of the $r \times r$ matrix $\tilde{A}$:

$$\tilde{A}R = R\Omega \qquad\qquad or \qquad\qquad \tilde{A} = R\Omega R^{-1}$$

where the columns of $r \times r$ matrix $R$ and diagonal matrix $\Omega$ respectively contain eigenvectors and their corresponding eigenvalues of $\tilde{A}$:

$$R = \begin{bmatrix} | & | & ... & | \\ \vec{r}_1 & \vec{r}_2 & ... & \vec{r}_r \\ | & | & ... & | \end{bmatrix} \qquad\qquad \Omega = \begin{bmatrix} w_1 & 0 & ... & 0 \\ 0 & w_2 & ... & 0 \\ 0 & 0 & ... & w_r \end{bmatrix}$$

Apply the eigendecomposition to our linear operator approximation:

$$U_m \approx AU_{m-1} = \Phi_r\tilde{A}\Phi_r^TU_{m-1} = \Phi_rR\Omega R^{-1}\Phi_r^TU_{m-1}$$

Here we define $n \times r$ matrix $F_{DMD} = \Phi_rR$, which has $r \times n$ pseudo-inverse matrix $F_{DMD}^{\dagger} = R^{-1}\Phi_r^{-1} = R^{-1}\Phi_r^T$, and rewrite the last equation:

$$U_m \approx \Phi_r R \Omega R^{-1} \Phi_r^T U_{m-1} = F_{DMD} \Omega F_{DMD}^{\dagger} U_{m-1}$$

Now the linear operator can be approximated by $A = F_{DMD} \Omega F_{DMD}^{\dagger}$. The so-called DMD modes $\vec{f}$ are columns of $n \times r$ matrix $F_{DMD}$:

$$F_{DMD} = \begin{bmatrix} | & | & \dots & | \\ \vec{f}_1 & \vec{f}_2 & \dots & \vec{f}_r \\ | & | & \dots & | \end{bmatrix}$$

After sorting the eigenvalues in $\Omega$ descendingly, we can plot the first 6 corresponding strongest DMD modes:

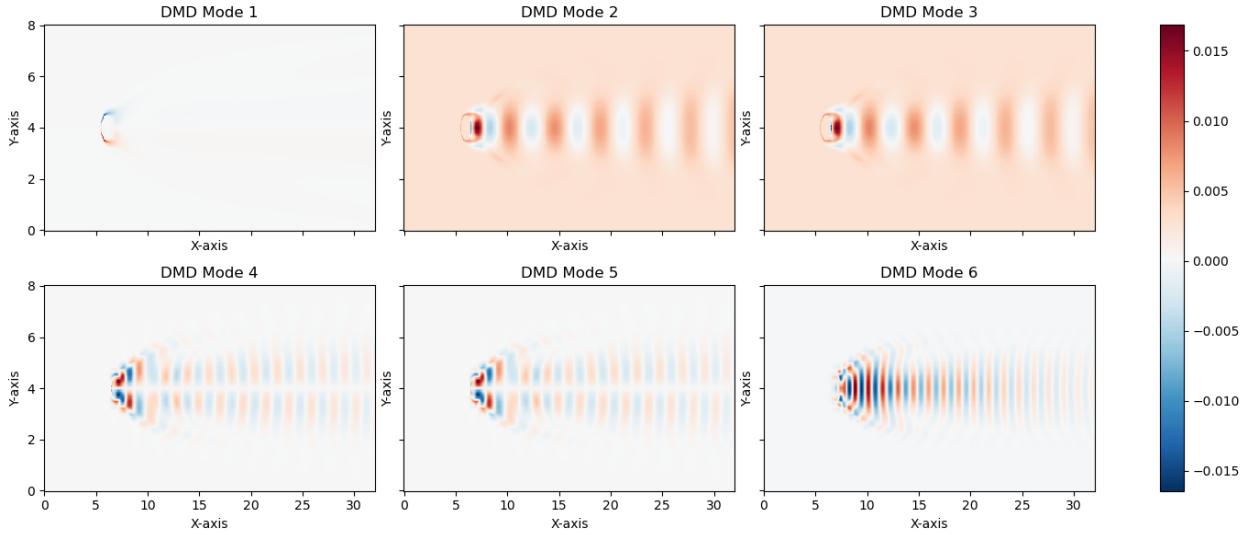


**Figure 6: Visualization of the First Six DMD Modes. The subplots display the spatial patterns of each DMD mode and the color represents the amplitude of the modes.**

With the DMD mode matrix $F_{DMD}$ and eigenvalue matrix $\Omega$ it is possible to reconstruct the state at discrete time $t_k$:

$$\vec{u}_k \approx A\vec{u}_{k-1} = F_{DMD} \Omega F_{DMD}^{\dagger} \vec{u}_{k-1} = F_{DMD} \Omega^{k-1} F_{DMD}^{\dagger} \vec{u}_1 = F_{DMD} \Omega^{k-1} \vec{b}$$

where $r \times 1$ column vector $\vec{b} = F_{DMD}^{\dagger} \vec{u}_1$, and use the eigenvalue $w_j$ of diagonal matrix $\Omega$ to continue write:

$$\vec{u}_k \approx F_{DMD}\Omega^{k-1}\vec{b} = \sum_{j=1}^{r} \vec{f}_j w_j^{k-1} b_j$$

The spectral expansion above can also be written in continuous time by introducing the continuous eigenvalues $w'_j = ln(w_j)/\Delta t$, so that:

$$w_j = e^{w'_j \Delta t}$$

$$w_j^{k-1} = e^{w'_j (k-1)\Delta t} = e^{w'_j t_k}$$

Then we can shift the $t_k$ to continuous time $t$, and rewrite the equation for approximating $\vec{u}_k$:

$$\vec{u}_k \approx \sum_{j=1}^{r} \vec{f}_j w_j^{k-1} b_j = \sum_{j=1}^{r} \vec{f}_j e^{w'_j t_k} b_j \approx \sum_{j=1}^{r} \vec{f}_j e^{w'_j t} b_j = F_{DMD} e^{\Omega t} \vec{b}$$

DMD is known to be extremely sensitive to noisy data, and this sensitivity can manifest in the eigenvalues. Noise in the data can introduce inaccuracies in the eigenvalue estimates, potentially leading to spurious modes and affecting the overall quality of the decomposition. The following graph plotting the eigenvalues on the complex plane provides a visual means to assess the impact of noise:

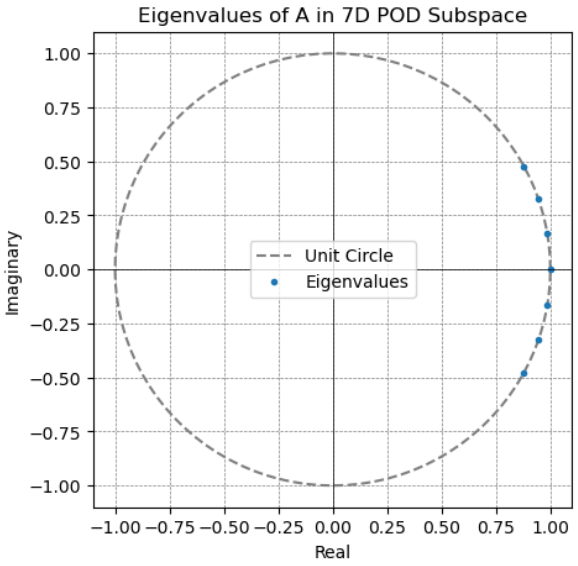


Figure 7: Distribution of 7-Dimensional DMD Eigenvalues on the Complex Plane

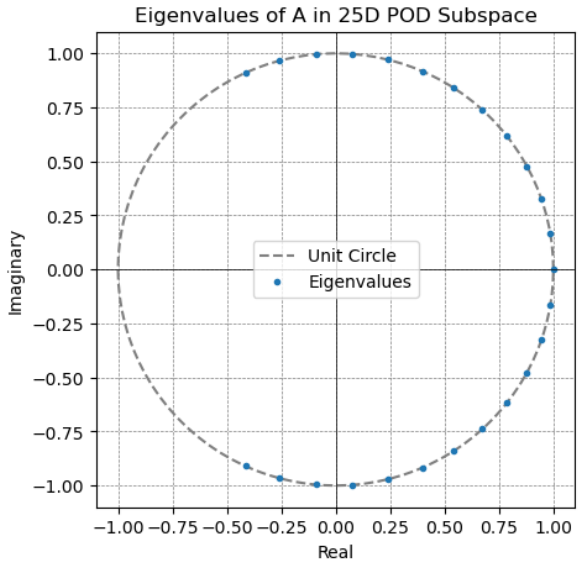


Figure 8: Distribution of 7-Dimensional DMD Eigenvalues on the Complex Plane

As we can tell from the above graph, all the eigenvalues for 7-dimensional and 25-dimensional projection are on the unit circle respectively, which means this dynamic system is stable and its dominant modes are well-defined and separated from noise. These eigenvalues are also symmetric with respect to the real axis, it may suggest robust modes.

The following scatter plot shows the values from one snapshot (at time-step 500) of the original data matrix $U$ against the corresponding snapshot from the 7-dimensional DMD reconstruction $\vec{u}_k$ and 25-dimensional DMD reconstruction $\vec{u}_k$ respectively:

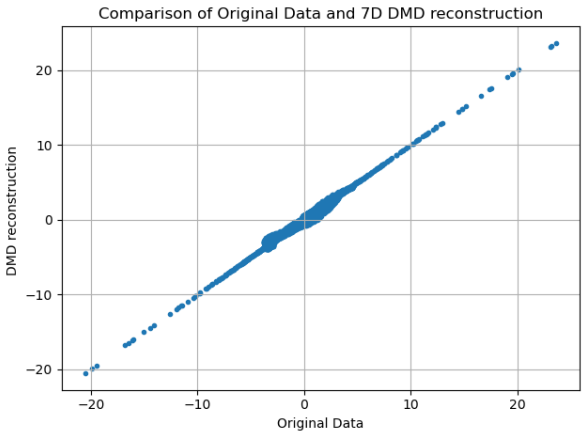


Figure 9(a): Original Data vs. 7-Dimensional DMD reconstruction at Time-Step 500

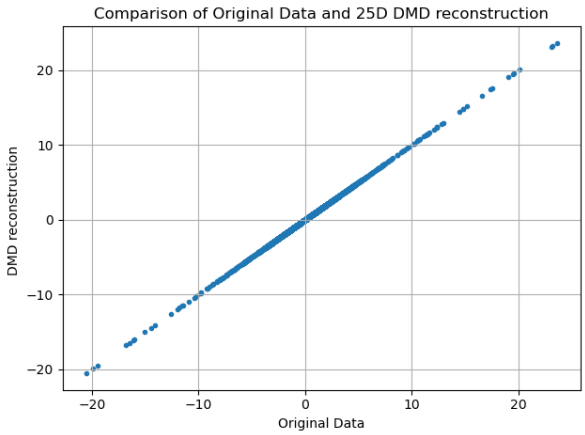


Figure 9(b): Original Data vs. 25-Dimensional DMD reconstruction at Time-Step 500

The result of Pearson's correlation coefficient $r_p$ between the original data $U$ and 7-dimensional DMD reconstruction $\vec{u}_k$ at 500-th snapshot is 0.99502526, which is slightly less than that of 7-rank POD approximation (0.9950573), but it is also close to 1, indicating a strong positive correlation, and meaning that $n \times 7$ matrix $F_{DMD}$ well captured the key pattern in the original data. The following graph visualizes the vorticity field of the original data at 500-th snapshot and the reconstructed vorticity field using the reduced-dimensional DMD model:

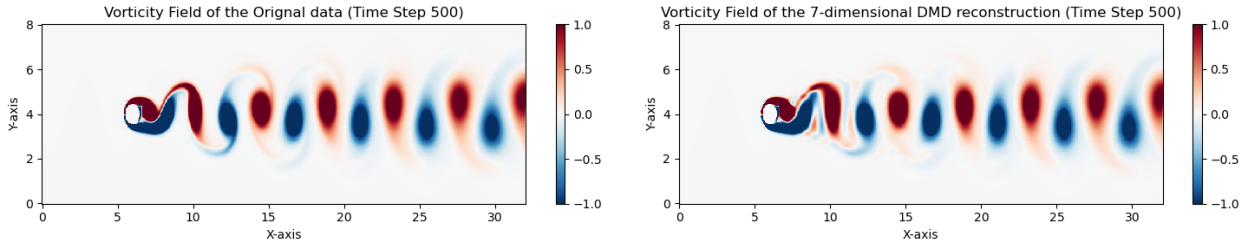


**Figure 10: Comparison of Vorticity Fields Between Original Data and the 7-dimensional DMD Reconstruction at 500 time-step**

If we chose to project A on the 25-dimensional POD subspace and conduct 25-dimensional DMD reconstruction, the result of Pearson's correlation coefficient $r_p$ between the original data $U$ and DMD reconstruction $\vec{u}_k$ at 500-th snapshot is 0.9999917, which is closer to 1, indicating a stronger positive correlation, and meaning that $n \times 25$ matrix $F_{DMD}$ captures the key pattern better. The following graph visualizes the vorticity field of the original data at the 500-th snapshot and the reconstructed vorticity field using the reduced-dimensional DMD model:

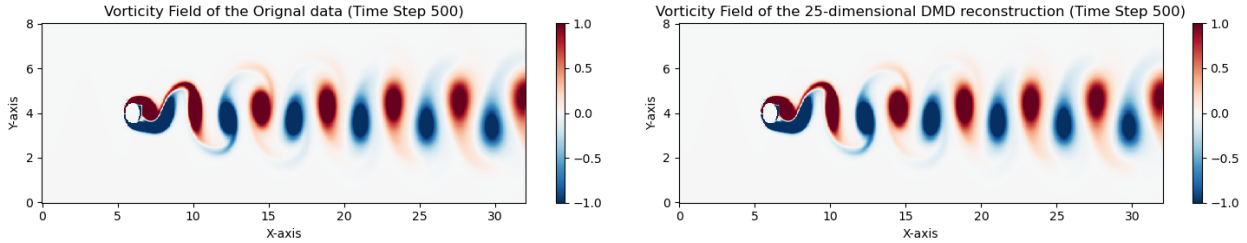


**Figure 11: Comparison of Vorticity Fields Between Original Data and the 25-dimensional DMD Reconstruction at 500 time-step**

# Conclusion

This project has successfully derived and applied POD and DMD methods to analyze dynamic systems, specifically the vorticity field of a two-dimensional fluid flow. We have captured coherent structures through POD and DMD modes and visualized dynamic structures. The detailed analysis of Pearson's correlation coefficient for a specific snapshot further validated the accuracy of POD approximation and DMD reconstruction compared to the original data. Moreover, the comparative assessments through scatter graphs have shown the data distributions, offering a nuanced view of the performance of POD and DMD methods. The conclusive comparison of reduced-rank POD approximation and reduced-dimensional DMD reconstruction with the original data at a specific snapshot presents the effectiveness of these reduced-order models in capturing the essential features of the studied dynamic system.

Autoencoders are neural network architectures designed for learning meaningful representations of input data. They consist of an encoder that maps the input to a lower-dimensional representation and a decoder that reconstructs the input from this representation. The encoder, in essence, learns to extract important features.  Analog to Encoder-Decoder Architecture in machine learning, the POD method can be viewed as a spatial autoencoder for extracting spatially coherent flow features from high-dimensional fluid data. It captures the essential features of the input data in a reduced-dimensional space. The decoder part reconstructs the input from this reduced representation.

DMD can be seen as a machine-learning framework tailored for fluid dynamics, and due to its regressive nature, it follows the memory architecture of neural network. In its application for this project, DMD efficiently captures and represents the system's evolving modes, offering a perspective on temporal dynamics. This analogy indicates the predictive capabilities of DMD, so applying the DMD method to machine learning of fluid dynamic systems is reasonable.

# Reference

[1] Scherl, I., Strom, B., Shang, J. K. (2020). "Robust principal component analysis for modal decomposition of corrupt fluid flows," *Physical Review Fluids*, **5**, 054401.

[2] Dai, X., Xu, D., Zhang, M., Stevens, R. J. A. M. (2022). "A three-dimensional dynamic mode decomposition analysis of wind farm flow
aerodynamics,"
*Renewable Energy*, **191**, 608-624.

[3] Notes and codes written by Dr. Jahrul Alam (alamj@mun.ca)